

1 **Non-stationary teleconnection between the Pacific**
2 **Ocean and Arctic sea ice**

3 **D.B. Bonan¹ and E. Blanchard-Wrigglesworth²**

4 ¹Environmental Science and Engineering, California Institute of Technology, Pasadena, CA, USA

5 ¹Department of Atmospheric Sciences, University of Washington, Seattle, WA, USA

6 **Key Points:**

- 7 • An observed teleconnection between Pacific Ocean SSTs and Arctic sea-ice extent is
8 analyzed in 30 fully-coupled GCMs participating in CMIP5
- 9 • Summer SST anomalies in the Pacific Ocean modulate September Arctic sea-ice ex-
10 tent through changes in upper Arctic air conditions
- 11 • This teleconnection is found to be non-stationary on multidecadal timescales both in
12 the GCMs able to simulate it and in observations

Corresponding author: David B. Bonan, dbonan@caltech.edu

13 **Abstract**

14 Over the last 40 years observations show a teleconnection between summertime Pacific
15 Ocean sea-surface temperatures and September Arctic sea-ice extent. However, the short
16 satellite observation record has made it difficult to further examine this relationship. Here,
17 we use 30 fully-coupled general circulation models (GCMs) participating in Phase 5 of the
18 Coupled Model Inter-comparison Project to assess the ability of GCMs to simulate this
19 teleconnection and analyze its stationarity over longer timescales. GCMs can temporarily
20 simulate the teleconnection in continuous 40-year segments, but not over longer, centennial
21 timescales. Each GCM exhibits considerable teleconnection variability on multidecadal
22 timescales. Further analysis shows the teleconnection depends on an equally non-stationary
23 atmospheric bridge from the subequatorial Pacific Ocean to the upper Arctic troposphere.
24 These findings indicate the modulation of Arctic sea ice by variability from the subequatorial
25 Pacific is not fixed in time, undermining the assumption of teleconnection stationarity as
26 defined by the satellite record.

27 **Plain Language Summary**

28 Understanding the processes leading to Arctic sea ice change remains a central goal in cli-
29 mate science. These changes affect not only weather and climate, but also local ecosystems,
30 indigenous populations, and socio-economic activities in the region. Recent studies have
31 shown that during the summer months, the Pacific Ocean influences Arctic sea ice. Such a
32 relationship suggests that this region of the Pacific Ocean may be a key source of predictabil-
33 ity for Arctic sea ice, especially for the summer minimum. However, our understanding of
34 this relationship is derived from a short observational record, which makes it difficult to
35 study how this relationship evolves over time. To overcome this limitation, we use long
36 simulations from 30 different global climate models. We show that models are able to sim-
37 ulate this relationship, but the relationship changes considerably over time. This suggests
38 the observed link between the Pacific Ocean and Arctic sea ice may change in the coming
39 decades; therefore, caution should be applied when forecasting or reconstructing Arctic sea
40 ice and assuming that this relationship is constant in time.

41 **1 Introduction**

42 Sea ice is a major component of the Arctic environment. It shapes the local ecosystems
43 (Wyllie-Echeverria & Wooster, 1998), the life of indigenous populations (Ford & Smit, 2004),

44 and the level of socio-economic activities in the region (Pizzolato et al., 2016; Melia et al.,
45 2016). Over the last few decades, satellite observations have revealed that Arctic sea ice has
46 undergone striking changes, a significant fraction of which is attributed to anthropogenic
47 climate change (e.g., Kay et al., 2011; Ding et al., 2019). There has been a sharp decline in
48 sea-ice extent, especially in summer and fall (Stroeve et al., 2007; Serreze et al., 2007; Comiso
49 et al., 2008; Serreze & Meier, 2018), substantial thinning across all months (Rothrock et
50 al., 1999; Kwok & Rothrock, 2009), and a notable loss of multiyear ice (Johannessen et al.,
51 1999; Rigor & Wallace, 2004; Maslanik et al., 2011). Given the importance of Arctic sea ice,
52 these changes have motivated a widespread effort to better understand the predictability of
53 Arctic sea ice (e.g., Eicken, 2013; Jung et al., 2016).

54 A quantitative picture of Arctic sea-ice predictability is beginning to emerge. Studies
55 on potential predictability in fully-coupled general circulation models (GCMs; e.g., Holland
56 et al., 2011; Blanchard-Wrigglesworth, Bitz, & Holland, 2011; Day, Tietsche, & Hawkins,
57 2014; Tietsche et al., 2014; Bushuk et al., 2019) and statistical and dynamical forecast
58 systems (e.g., W. Wang et al., 2013; Merryfield et al., 2013; Sigmond et al., 2013; Chevallier
59 et al., 2013; Msadek et al., 2014; Blanchard-Wrigglesworth et al., 2015; Guemas et al., 2016;
60 L. Wang et al., 2016; Petty et al., 2017; Bushuk et al., 2017) have shown that forecasts
61 of pan-Arctic sea-ice extent (SIE) may be skillful anywhere between 2 months and 2 years
62 in advance. At regional scales — which is often more societally relevant — dynamical
63 prediction systems can skillfully predict SIE on seasonal timescales (Bushuk et al., 2017) or
64 even decadal timescales (Yeager et al., 2015). While these results are certainly promising,
65 more recent work has shown that prediction skill for regional summer SIE drops significantly
66 for forecasts initialized prior to May (Bushuk et al., 2017, 2019), possibly limiting accurate
67 summer forecasts for stakeholders. The existence of this “spring predictability barrier” is
68 also found to be remarkably robust across dynamical models, with all GCMs participating in
69 phase 5 of the Coupled Model Intercomparison Project (CMIP5) displaying a predictability
70 barrier structure in late spring (Bonan, Bushuk, & Winton, 2019). This barrier, along
71 with mounting evidence for a significant gap between the potential and operational forecast
72 skill of Arctic SIE (Blanchard-Wrigglesworth et al., 2015; Bushuk et al., 2019) and the
73 possibility that GCMs may overestimate sea-ice predictability (Blanchard-Wrigglesworth &
74 Bushuk, 2019), motivates the need to better understand physically-based mechanisms for
75 Arctic sea-ice predictability. An improved understanding may improve operational forecasts.

76 For summer Arctic sea ice, in particular, considerable effort has gone toward identifying
77 such mechanisms. Numerous variables have been found to offer information on prediction
78 skill, including: sea-ice thickness (Blanchard-Wrigglesworth, Armour, et al., 2011; Day,
79 Hawkins, & Tietsche, 2014; Dirkson et al., 2017; Bushuk et al., 2017; Bonan, Bushuk, &
80 Winton, 2019), sea-ice motion in the winter (Williams et al., 2016), melt pond fraction in
81 the spring (Schröder et al., 2014), ocean heat fluxes (Woodgate et al., 2010), stratospheric
82 conditions (Smith et al., 2018), longwave radiation in the spring (Kapsch et al., 2013), sur-
83 face winds (Ogi et al., 2010), and tropospheric temperatures in the summer (Ding et al.,
84 2017). Remote processes have also been found to impact summer Arctic sea ice. Summer
85 tropical Pacific sea surface temperatures (SSTs), for instance, modulate interannual changes
86 in the Arctic environment via atmospheric wave propagation (Ding et al., 2014; Hu et al.,
87 2016; Ding et al., 2019; Baxter et al., 2019). The preferred circulation response or “at-
88 mospheric teleconnection” to a particular SST pattern results from a large-scale barotropic
89 Rossby wave train that causes interactions between the mean flow anomaly and transient
90 eddies (see review by Trenberth et al., 1998). Throughout the year, numerous atmospheric
91 teleconnections can influence Arctic sea ice (L’Heureux et al., 2008; Screen & Francis, 2016;
92 Meehl et al., 2018; Ding et al., 2019; Screen & Deser, 2019; Baxter et al., 2019; Castruccio
93 et al., 2019). For example, Baxter et al. (2019) show that cool SST anomalies in the sube-
94 quatorial Pacific Ocean leads to reduced local convection, which generates anomalous upper
95 level divergence that, in turn, creates a barotropic Rossby wave train propagation from the
96 tropical Pacific Ocean to the Arctic. Referred to as the “Pacific-Arctic (PARC) telecon-
97 nection”, this wave train favors persistent positive geopotential height anomalies centered
98 over northeastern Canada and Greenland that cause warmer tropospheric temperatures and
99 reduced sea ice. Since it is thought the PARC teleconnection has contributed to accelerated
100 Arctic sea ice loss in recent years (Baxter et al., 2019), it is crucial to quantify the ability of
101 GCMs to correctly simulate it and to assess its stationarity, given the short satellite obser-
102 vation record. Such quantification may impact assessments of Arctic sea-ice predictability
103 on seasonal-to-interannual timescales.

104 Indeed, recent work has shown that in a CMIP5 GCM (CESM1-CAM5) the tropics have
105 a modest impact on seasonal forecast skill for Arctic sea ice (e.g., Blanchard-Wrigglesworth
106 & Ding, 2019), which suggests less of a role for tropical teleconnections. Yet, this result is
107 contingent on the GCM correctly simulating teleconnections to the Arctic from the tropics.
108 If a particular GCM does not simulate the correct tropical-polar linkage, remote prediction

109 skill may be underestimated. It has been noted, for instance, that CESM1-CAM5 does
110 not replicate the PARC teleconnection well enough (Baxter et al., 2019). However, it re-
111 mains unknown whether this is because of model bias or internally-generated variability
112 (Blanchard-Wrigglesworth & Ding, 2019). Likewise, there is growing evidence that tele-
113 connections can shift both in space and time over decadal and centennial timescales (e.g.,
114 Coats et al., 2013; Raible et al., 2014; Batehup et al., 2015; Dätwyler et al., 2018; Kolstad
115 & Screen, 2019). But because of the temporally-limited satellite observation record, it is
116 difficult to quantify the stationarity of the PARC teleconnection. These issues raise two im-
117 portant questions that we address in this work: (i) do GCMs simulate the observed PARC
118 teleconnection and (ii) how robust and stationary is the PARC teleconnection?

119 Using output from 30 CMIP5 models, we evaluate the skill of GCMs in simulating the
120 PARC teleconnection and characterize its stationarity on decadal and centennial timescales.
121 We first discuss the PARC teleconnection between summertime SSTs and September Arctic
122 SIE in the satellite observation record (1979–2018). We then compute this relationship
123 across unforced control simulations in CMIP5 and show that GCMs can simulate the PARC
124 teleconnection over 40-year periods, but not over longer, centennial timescales. Finally, using
125 continuous 40-year segments from the unforced control simulations, we demonstrate that
126 GCMs exhibit considerable PARC teleconnection variability on multidecadal timescales.

127 **2 Data**

128 **2.1 Observational datasets**

129 For observation-based data of the geopotential height at 200 hPa (Z200), we use the
130 NCEP-NCAR reanalysis (Kalnay et al., 1996). For SST data over the observation period, we
131 use the Hadley Centre’s sea ice and sea surface temperature (HadISST.2) dataset (Rayner
132 et al., 2003). Note, this analysis is insensitive to the choice of reanalysis dataset (e.g., ERA-
133 Interim). We regrid both fields to a $1.0^\circ \times 1.0^\circ$ analysis grid using the nearest-neighbor
134 interpolation. Since regridding can result in differences from the original grid (Hofstra et al.,
135 2008), we compare the adjusted and original grid and find little difference. Monthly Arctic
136 SIE from 1979 to 2018 was derived using observations of monthly sea-ice concentration
137 (SIC) from the National Snow and Ice Data Center (NSIDC) passive microwave retrievals
138 bootstrap algorithm (Comiso et al., 2017). We also use a reconstruction of monthly Arctic

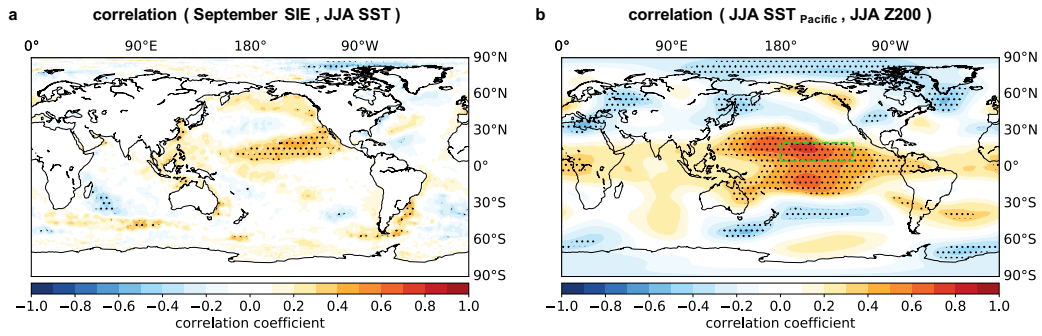
139 SIE from 1953 (Walsh et al., 2017) to analyze teleconnection stationarity over a longer
140 observation period.

141 **2.2 CMIP5 output**

142 To analyze teleconnection stationarity over longer time periods, we use monthly out-
143 put from 30 different GCMs participating in CMIP5 (Taylor et al., 2012). We use the
144 preindustrial control, historical, and RCP8.5 simulations. Since the historical simulations
145 end in 2005, to produce a 1979–2018 “satellite observation period” for CMIP5, we merge
146 the 1979–2005 fields from the historical simulations with the 2006–2018 fields under the
147 RCP8.5 forcing scenario (hereafter referred to as “historical-RCP8.5”). At such short time
148 scales and so early in the 21st century, the uncertainty associated with choice of forcing
149 scenario is negligible (Hawkins & Sutton, 2009). For each experiment, we consider three
150 quantities: SIC, SST, and Z200. The set of GCMs evaluated for all three quantities reflect
151 those that provide the necessary output (see Table S1). All model output is regridded to a
152 common $1^\circ \times 1^\circ$ analysis grid using nearest-neighbor interpolation. With each GCM, we
153 compute monthly Arctic SIE (defined as the area where $\text{SIC} > 15\%$) over 1979–2018 and the
154 200-year-long preindustrial control run.

155 **3 The Pacific Ocean teleconnection to Arctic sea ice in observations** 156 **(1979–2018)**

164 We begin by quantifying the PARC teleconnection in observations (1979–2018) through
165 correlation maps analogous to the teleconnection measure used in Wallace and Gutzler
166 (1981). Figure 1a shows the correlation map between global June, July, and August (JJA)
167 SSTs and September Arctic SIE from 1979 to 2018. Note, both datasets were linearly de-
168 trended prior to correlation calculations. Over the satellite observation period, there is a
169 modest, but statistically significant (at the 95% confidence level) positive correlation situ-
170 ated in the subequatorial Pacific and the eastern branch of the Pacific Decadal Oscillation
171 (PDO). Such a relationship suggests that positive summertime SST anomalies in the Pacific
172 Ocean is related to positive Arctic SIE anomalies in September. To investigate a causal
173 mechanism, we analyze if there exists an atmospheric bridge linking the two variables. Fig-
174 ure 1b shows the correlation map between JJA SST averaged over the tropical Pacific region
175 that shows highest SST correlations with Arctic SIE (5°N to 20°N and 180° to 90°W , see
176 green dashed box in Fig. 1b) and global JJA Z200 from 1979 to 2018. Again, both datasets

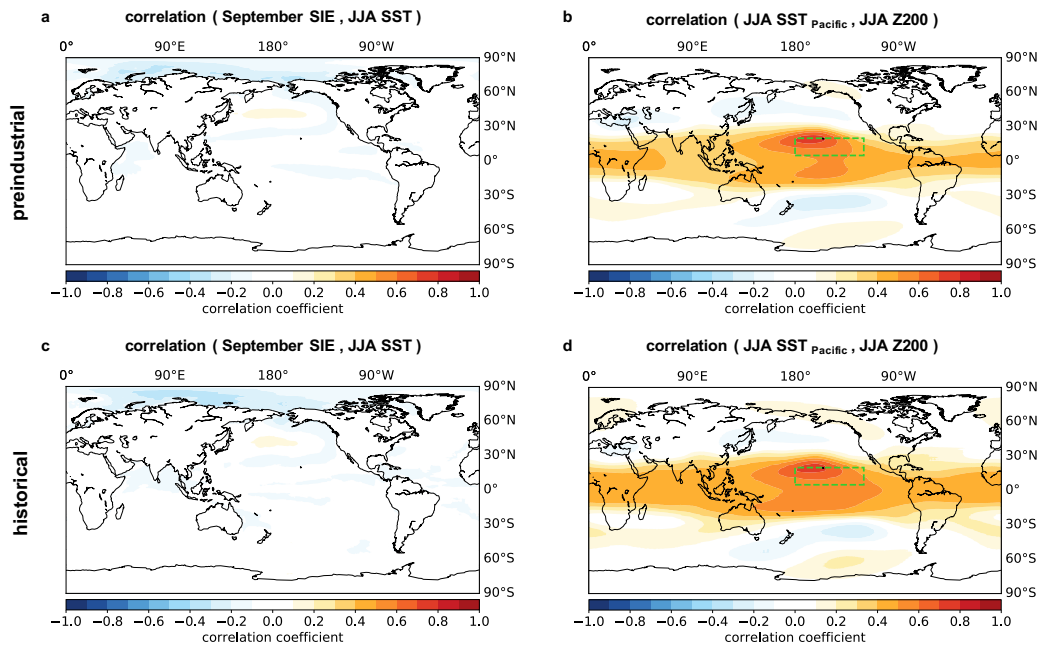


157 **Figure 1.** The Pacific Ocean teleconnection to Arctic sea ice in observations (1979–2018). (a)
 158 Pearson correlation coefficient between September Arctic sea-ice extent (SIE) and global June,
 159 July, and August (JJA) sea surface temperatures (SSTs) from 1979–2018. (b) Pearson correlation
 160 coefficient between JJA SST averaged in the dashed green box and global JJA 200 hPa geopotential
 161 height (Z200) from 1979–2018. Black dots denote statistically significant correlation coefficient
 162 values at the 95% confidence level. All datasets are linearly detrended before correlation coefficient
 163 values are calculated.

177 were linearly detrended before correlation calculations. Figure 1b shows a statistically sig-
 178 nificant (at the 95% confidence level) area of negative Z200 correlations throughout the
 179 Arctic, with the largest negative correlation coefficient values occurring in the Central Arc-
 180 tic, Canadian Archipelago, Baffin Bay, and Labrador Sea. This correlation suggests that
 181 positive SST anomalies in the subequatorial Pacific Ocean generate negative Z200 anoma-
 182 lies throughout the Arctic — which is consistent with cooler tropospheric temperatures and
 183 favorable conditions for positive September Arctic SIE anomalies (Ding et al., 2019; Baxter
 184 et al., 2019; Olonscheck et al., 2019). This result is also consistent with previous work that
 185 has identified similar correlation structures for glacier mass-balance anomalies in the region
 186 (e.g., Bonan, Christian, & Christianson, 2019).

187 **4 The Pacific Ocean teleconnection to Arctic sea ice in CMIP5**

194 We now turn to output from GCMs participating in CMIP5 by first computing the
 195 teleconnection relationship in the preindustrial control simulations. Figure 2a shows the
 196 ensemble mean correlation map computed between global JJA SSTs and September Arctic
 197 SIE over the 200-year-long preindustrial control run from all 30 GCMs. For each GCM,
 198 both datasets were linearly detrended prior to the calculations. Across the entire suite,



188 **Figure 2.** The Pacific Ocean teleconnection to Arctic sea ice in CMIP5. The ensemble mean
 189 correlation map between September Arctic sea-ice extent (SIE) and global June, July, and August
 190 (JJA) sea surface temperatures (SSTs) across all 30 GCMs using the (a) preindustrial control and
 191 (c) historical-RCP8.5 (1979–2018) simulations. The ensemble mean correlation map between JJA
 192 SST averaged in the dashed green box and global JJA 200 hPa geopotential height (Z200) across
 193 all 30 GCMs using the (b) preindustrial control and (d) historical-RCP8.5 (1979–2018) simulations.

199 not a single GCM simulates the observed spatial features in the Pacific Ocean (see Fig.
200 S1). Notably, some of the GCMs (~ 11) simulate the opposite relationship, with negative
201 correlations between JJA SSTs and September Arctic SIE in the subequatorial Pacific (see
202 e.g., BCC-CSM1.1(m) in Fig. S1). Additionally, the observed tropical-polar SST-Z200
203 linkage is not simulated. Figure 2b shows the the ensemble mean correlation map computed
204 between JJA SST averaged over 5°N to 20°N and 180° to 90°W (i.e., the dashed green
205 box) and global JJA Z200 over the 200-year-long preindustrial control run from all 30
206 GCMs. While GCMs generally agree in showing large positive correlations across the tropics
207 and a Rossby wave train over the southeastern Pacific Ocean and Southern Ocean, not a
208 single GCM replicates the negative Z200 correlations in the Arctic (see Fig. S2), as seen
209 in the observations (see Fig. 1b). Interestingly, BCC-CSM1.1(m), which simulates the
210 strongest SIE-SST relationship opposite to observations (i.e., negative SST correlations in
211 the subequatorial Pacific Ocean), produces a positive correlation between JJA Pacific SST
212 and JJA Z200 in the Arctic (see Fig. S2), which is also opposite to the observed relationship.

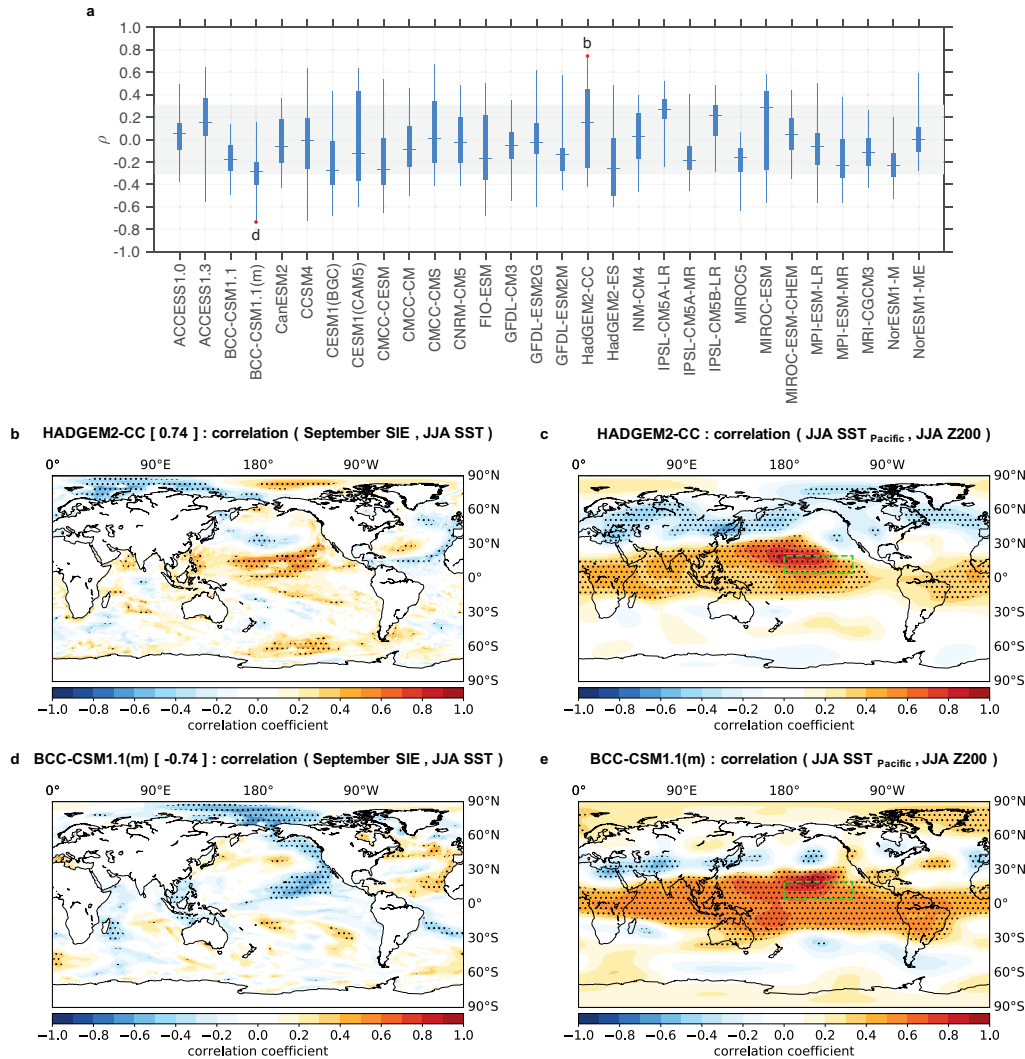
213 The above analysis is computed across 200-year-long unforced control simulations. To
214 investigate if the teleconnection is only present at shorter timescales and under modern day
215 conditions, we compute the PARC teleconnection in the CMIP5 historical-RCP8.5 simula-
216 tions. Figure 2c shows the ensemble mean correlation map computed between global JJA
217 SSTs and September Arctic SIE over 1979–2018 from all 30 GCMs (after linearly detrending
218 all variables). Despite using a 40-year time period — which is substantially shorter than
219 the 200-year-long preindustrial control run — most GCMs do not accurately simulate the
220 observed teleconnection (see Fig. S3). Similarly, the crucial atmospheric bridge that links
221 the Pacific Ocean to Arctic sea ice is absent. Figure 2d shows the the ensemble mean corre-
222 lation map computed between JJA SST averaged over 5°N to 20°N and 180° to 90°W (i.e.,
223 the green box) and global JJA Z200 over 1979–2018 from all 30 GCMs. GCMs show robust
224 positive correlation values throughout the tropics and a Rossby wave train to the Southern
225 Ocean, but again struggle to simulate a negative relationship in the Arctic. Notably, while
226 the ensemble mean correlation map lacks the statistically-significant negative Z200 correla-
227 tion structure over the Arctic, CMCC-CMS — which most closely resembles the observed
228 teleconnection pattern (i.e., Fig. 1a) — does indeed simulate the linkage (see Fig. S3 and
229 S4), with negative Z200 correlation values throughout the Arctic. This result lends credence
230 that GCMs may indeed be able to simulate this relationship.

4.1 Multidecadal teleconnection variability

The inability of GCMs to simulate the observed PARC teleconnection suggests that either model bias is impacting the relationship between the Pacific Ocean and Arctic sea ice, or that there is significant internal variability in the evolution of this teleconnection and observations sample an extreme realization. For instance, Blanchard-Wrigglesworth and Ding (2019) note that although the ensemble mean of 40 large ensemble members in CESM1(CAM5) fails to simulate the Pacific Ocean teleconnection to Arctic sea ice, individual ensemble members are able to simulate the correct relationship, which suggests a role for internal variability.

To investigate teleconnection stationarity over longer timescales, the preindustrial control simulations were divided into continuous 40-year segments to match the length of the satellite observation record (1979–2018), generating a set of 160 segments for each control run. For each segment, the correlation map between September Arctic SIE and JJA SSTs was calculated and compared to the observed correlation map (see Fig. 1a), by determining the pattern correlation, ρ , between the two correlation maps. Before the pattern correlation values were determined we restricted the spatial domain of both the observational map (i.e., Fig. 1a) and each map of the 160 segments from 0° to 65°N and 90°E to 90°W since the north Pacific Ocean is the primary region of interest. As noted by Raible et al. (2014), the pattern correlation is a strict skill metric, where even a spatial pattern offset by a two grid points will cause the pattern correlation value, ρ , to deteriorate from $\rho = 1.0$ to approximately $\rho = 0.85$. The range in pattern correlation values is thus interpreted as a measure of the temporal stationarity of the teleconnection for a given GCM.

The pattern correlation values, ρ , for each GCM are shown in Figure 3a. The mean for all GCMs falls below the significance threshold (~ 0.31 ; see grey shading in Fig. 3a), and is thus statistically indistinguishable from a correlation value of 0.0. This result is consistent with the correlation maps from the 200-year-long unforced control simulations, which show little-to-no teleconnection (see Fig. 2a). It also suggests that the PARC teleconnection is often inactive. Notably, the GCMs (e.g., BCC-CSM1.1(m)) with mean negative correlation values ($\bar{\rho} < 0$) are also the GCMs whose 200-year-long correlation map tended toward an opposite relationship to observations (see Fig. S1). Furthermore, some GCMs (e.g., BCC-CSM1.1, BCC-CSM1.1(m), and MIROC5) show less variability in the teleconnectivity, while others (e.g., CCSM4, CESM1(CAM5), and HadGEM2-CC) exhibit a considerable range of



253 **Figure 3.** Illustration of variability in the Pacific Ocean teleconnection to Arctic sea ice. (a)
 254 Pacific Ocean teleconnection stationarity, as measured by the pattern correlation, ρ , of the North
 255 Pacific Ocean (0° to 65°N , 90°E to 90°W), using the Pacific Ocean teleconnection map estimated
 256 from observations (Fig. 1a) and continuous 40-year segments from the 200-year-long preindustrial
 257 control simulations. Box plots indicate the 25th and 75th percentile of the pattern correlation
 258 statistic across the segments in each respective GCM with the mean as the central line and the
 259 whiskers showing the full data range. The grey shading represents the bounds of statistically-
 260 significant values at the 95% confidence level. The letters denote the correlation map for (b) and
 261 (d). The Pacific Ocean teleconnection map from the most positive pattern correlation value (Fig.
 262 3b) and the most negative pattern correlation value (Fig. 3d), respectively, and the corresponding
 263 SST-Z200 correlation map (Fig. 3c and Fig. 3e). The bracketed numbers in Fig. 1b and Fig. 1d
 264 are the pattern correlation values with the observed teleconnection map.

275 pattern correlation values. Although such a large inter-model spread exists in the ability
276 of GCMs to simulate this teleconnection, we focus here on the ability of GCMs to simulate
277 the relationship during any given 40-year segment.

278 Figure 3b shows the correlation map of global JJA SSTs and September Arctic SIE for
279 the GCM with the most positive pattern correlation value (i.e., HadGEM2-CC, $\rho = 0.74$)
280 and Figure 3d shows the correlation map of global JJA SSTs and September Arctic SIE for a
281 GCM with the most negative pattern correlation value (i.e., BCC-CSM1.1(m), $\rho = -0.74$).
282 In Fig. 3b a statistically-significant positive correlation is situated in the subequatorial
283 Pacific Ocean, almost identical to observations. Furthermore, the atmospheric bridge (i.e.,
284 the correlation map between JJA Pacific SST and global JJA Z200) shows a statistically-
285 significant (at the 95% confidence level) negative correlation value off the coast of Greenland
286 and over the Canadian Archipelago (see Fig. 3c). Conversely, BCC-CSM1.1(m) shows a
287 statistically-significant (at the 95% confidence level) region of negative correlation in the
288 subequatorial Pacific Ocean (see Fig. 3d). Similarly, the atmospheric bridge, which is
289 the correlation map between JJA Pacific SST and global JJA Z200, shows a statistically-
290 significant positive correlation region over Greenland and the Barents Sea (see Fig. 3e).
291 While this result suggests some GCMs are capable of simulating the teleconnection between
292 the Pacific Ocean and Arctic sea ice, there is significant spread, both in time and across
293 GCMs, in the simulated character of this teleconnection.

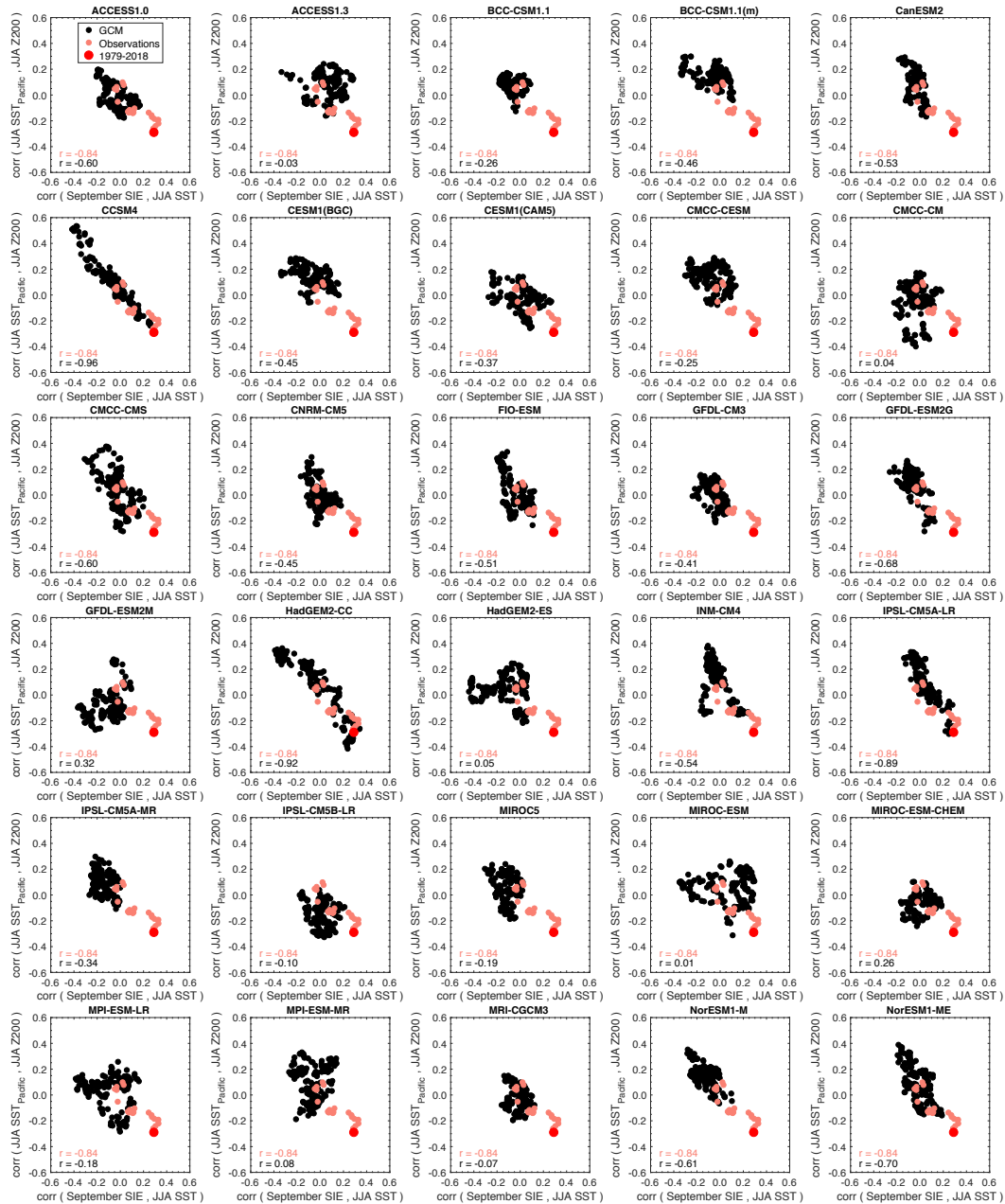
294 **4.2 Non-stationary atmospheric bridge**

295 Even within a single GCM, there is considerable variability in the simulated character
296 of the PARC teleconnection over multidecadal timescales. This non-stationarity leads us
297 to ask how stationary is the atmospheric bridge linking the Pacific Ocean to Arctic sea
298 ice? Following from the previous 40-year segment analysis, the set of 160 segments for each
299 control run was used to compute the correlation between JJA Pacific SST (the green box)
300 and global JJA Z200. The correlation maps of each member were then averaged from 70°N
301 to 90°N and 180° to 90°W to capture the SST-Z200 relationship in the Arctic (see y -axis of
302 Fig. 4). Similarly, the SST-SIE correlation maps of each GCM (i.e., Fig. 3) were averaged
303 from 5°N to 20°N and 180° to 90°W to capture the SIE-SST relationship in the Pacific (see
304 x -axis of Fig. 4). The two values from all 160 slices across all 30 GCMs were then compared
305 to evaluate the relationship between strong positive correlations from JJA Pacific SST and

306 September Arctic SIE (i.e., the PARC teleconnection) and strong negative correlations from
307 JJA Pacific SST and JJA Z200 (i.e., the atmospheric bridge to the Arctic from the Pacific).

320 Figure 4 shows scatter plots of the relationship described above in each GCM. GCMs
321 tend to show two different behaviors: a cluster of values centered around 0.0 for both the SIE-
322 SST and SST-Z200 correlations, indicating that no PARC teleconnection is simulated (e.g.,
323 ACCESS1.3, CMCC-CM) and another cluster of values that show opposite correlation signs
324 during different periods, indicating that a PARC teleconnection is simulated (e.g., CCSM4,
325 HadGEM2-CC). As mentioned above, this means that during some periods, positive SST
326 anomalies in the Pacific Ocean lead to negative Z200 anomalies in the Arctic and positive
327 Arctic SIE anomalies. Interestingly, during other periods these same GCMs simulate an
328 opposite teleconnection to PARC: positive SST anomalies in the Pacific Ocean lead to
329 positive Z200 anomalies in the Arctic and negative Arctic SIE anomalies. This illustrates a
330 non-stationary teleconnection between the Pacific Ocean and Arctic sea ice in GCMs.

331 Can one assess the stationarity of the PARC teleconnection in observations? To analyze
332 this, we use a reconstruction of September Arctic SIE (Walsh et al., 2017) and HadISST.2
333 SSTs from 1953 to present. We then divide the record into 40-year segments beginning
334 in 1953. We select 1953 as this is when more extensive sea ice observations become avail-
335 able (Walsh et al., 2017). This produces a set of 26 segments and allows us to examine
336 teleconnection stationarity in observations. We then compute the correlation maps be-
337 tween JJA SST and September Arctic SIE and average over the correlation values from
338 5°N to 20°N and 180° to 90°W . Likewise, we compute the correlation maps between JJA
339 Pacific SST and JJA Z200 and average over the correlation values from 70°N to 90°N and
340 180° to 90°W . The light red dots show the range of correlation values in observations,
341 with the large dark red dot showing the relationship calculated over the satellite era (i.e.,
342 1979–2018). Notably, only the GCMs with large non-stationarity in the PARC telecon-
343 nection (e.g., CCSM4, HadGEM2-CC, IPSL-CM5A-LR, and NorESM1-ME) are within the
344 range of the satellite era PARC teleconnection (see large red dot). Conversely, some GCMs
345 (e.g., CMCC-CM, HadGEM2-ES, MIROC-ESM, MIROC-ESM-CHEM, MPI-ESM-MR, and
346 MRI-CGCM3) show little-to-no relationship (or the opposite relationship), suggesting that
347 some GCMs are unable to replicate the observed teleconnection linkage. However, this could
348 be due to the choice of averaging region; some GCMs may have a different region of maximal
349 correlation possibly due to model bias. Importantly, it becomes clear that during the earlier
350 parts of the observational record, the PARC teleconnection was not present (note the light



308 **Figure 4.** The relationship between the SIE-SST correlation values and SST-Z200 correlation
 309 values in each GCM. The x -axis shows the average correlation value over the region that shows
 310 highest SIE-SST correlations in the observed teleconnection pattern (5°N to 20°N , 180° to 90°W)
 311 using values from each of the continuous 40-year segments of the 200-year-long preindustrial control
 312 simulations. The y -axis shows the average correlation value over the region that shows highest SST-
 313 Z200 correlations in the observed teleconnection pattern (70°N to 90°N , 180° to 90°W) using values
 314 from each of the continuous 40-year segments of the 200-year-long preindustrial control simulations.
 315 The correlation between the variables of each GCM is shown in the bottom left corner of each plot.
 316 The light red dots show the same relationship using continuous 40-year segments from reanalysis
 317 datasets, where the large dark red dot is the observed teleconnection relationship in the satellite
 318 record (1979–2018). The correlation using the reanalysis datasets is also shown in the bottom left
 319 corner of each plot.

351 red dots clustered around 0.0). From 1953 to 1992, there are no statistically significant
352 correlation values in the Pacific Ocean (see Fig. S5). This suggests — as seen in the GCMs
353 that do temporarily simulate the observed teleconnection — the PARC teleconnection is
354 also non-stationary in the real world.

355 **5 Discussion and conclusions**

356 Understanding the processes leading to Arctic sea ice change allows us to better inter-
357 pret observed changes and better predict future changes. Recent studies have shown that
358 summertime SSTs in the subequatorial Pacific Ocean can affect September Arctic sea ice
359 through atmospheric wave propagation (e.g., Ding et al., 2019; Baxter et al., 2019). Indeed,
360 we find across the observational record (1979–2018) there are statistically significant corre-
361 lation coefficient values between September Arctic SIE and JJA SSTs in the subequatorial
362 Pacific Ocean (see Fig. 1a). In this region, positive JJA SST anomalies generate negative
363 JJA Z200 anomalies throughout the Arctic (see Fig. 1b), which is consistent with conditions
364 favorable for positive September Arctic SIE anomalies (Ding et al., 2019; Baxter et al., 2019;
365 Olonscheck et al., 2019). Referred to as the “Pacific-Arctic (PARC) teleconnection”, this
366 mode is thought to have — in conjunction with anthropogenic climate change — contributed
367 to Arctic sea ice loss in recent years (Baxter et al., 2019). Yet, much of our understanding of
368 this teleconnection is derived from a temporally-limited satellite observation record, which
369 means we may not fully understand how this teleconnection evolves over time. Furthermore,
370 GCMs may be unable to replicate the observed teleconnection (Blanchard-Wrigglesworth &
371 Ding, 2019; Baxter et al., 2019). To address these concerns, we used output from CMIP5
372 to evaluate the ability of GCMs to simulate this teleconnection and further characterize its
373 stationarity on decadal and centennial timescales.

374 By investigating this teleconnection across 200-year-long unforced control simulations,
375 we find that GCMs are unable to accurately simulate this teleconnection on centennial
376 timescales (Fig. 2a-b). Even on 40-year timescales that occur during the observed historical
377 period (1979–2018), we find most GCMs are unable to accurately simulate this teleconnec-
378 tion (Fig. 2c-d). However, by splitting the 200-year-long unforced control simulations into
379 continuous 40-year segments that match the length of the observational record, we show
380 that a minority of GCMs are able to temporarily simulate the observed teleconnection, but
381 these GCMs exhibit considerable variability on multidecadal timescales (see Fig. 3a). In
382 these GCMs, positive JJA SST anomalies in the subequatorial Pacific Ocean generate neg-

383 active JJA Z200 anomalies throughout the Arctic (Fig. 3b-c), but during other times the
384 reverse relationship is simulated, as positive JJA SST anomalies in the subequatorial Pacific
385 Ocean generate positive JJA Z200 anomalies throughout the Arctic (Fig. 3d-e). Since Z200
386 anomalies affect tropospheric temperatures in the Arctic (Ding et al., 2017, 2019; Baxter
387 et al., 2019), these Pacific Ocean SST anomalies modulate Arctic sea ice loss. A poten-
388 tial caveat to this assessment is the significant spread in the ability of GCMs to correctly
389 simulate the PARC teleconnection. These inter-model differences could be due to model
390 biases in SST variability in the subequatorial Pacific Ocean. For instance, a GCM with
391 weak SST variability in this region is likely to have insufficient variability in convection and
392 Rossby wave generation and hence a weaker teleconnection. Indeed, we find that GCMs
393 with lower pattern correlation values tend to have weaker Pacific SST variability, but the
394 variability is still within range of observations (see Fig. S6). While out of the scope of this
395 study, further characterizations of inter-model differences and teleconnection mechanisms
396 may improve our understanding of the PARC teleconnection behavior.

397 Our analysis suggests substantial variability in the simulated character of this telecon-
398 nection, with an equally non-stationary atmospheric bridge from the subequatorial Pacific
399 Ocean to the Arctic (see Fig. 4). Although this teleconnection is often dormant, large
400 decadal variability can give rise to rare multidecadal periods where the PARC teleconnec-
401 tion is active, like that seen from 1979–2018. Additionally, as evinced by the PARC tele-
402 connection not being present in the earlier part of the observational record (1953–1992), it
403 is plausible that the observed relationship between the Pacific Ocean and Arctic sea ice will
404 change in the coming decades. Given such clear non-stationarity, we caution use of statistical
405 reconstructions and predictions of Arctic sea ice using Pacific SST information. Statistical
406 models rely almost exclusively on fixed relationships between Arctic sea ice and predictor
407 variables, implying that the processes affecting Arctic sea ice do not change over time. On
408 the other hand, because dynamical models can simulate this non-stationary teleconnection,
409 GCMs may be useful tools to study the processes that give rise to non-stationarity. Better
410 understanding the origins of this non-stationarity will improve predictions and projections
411 of Arctic sea ice, possibly helping to inform us when the Arctic will be ice free.

412 **Acknowledgments**

413 This work benefited from insightful discussions with C.M. Bitz and J.M. Wallace. F.
414 Lehner provided helpful comments on teleconnection stationarity in the observational record.

415 We thank L.A. Parsons for detailed comments on a draft of this manuscript. We also
416 thank the climate modeling groups for producing and making available their model out-
417 put, which is accessible at the Earth System Grid Federation (ESGF) Portal ([https://esgf-
node.llnl.gov/search/cmip5/](https://esgf-
418 node.llnl.gov/search/cmip5/)).

419 **References**

- 420 Batehup, R., McGregor, S., & Gallant, A. (2015). The influence of non-stationary tele-
421 connections on palaeoclimate reconstructions of ENSO variance using a pseudoproxy
422 framework. *Climate of the Past*, *11*(12), 1733–1749.
- 423 Baxter, I., Ding, Q., Schweiger, A., LHeureux, M., Baxter, S., Wang, T., . . . Lu, J. (2019).
424 How tropical Pacific surface cooling contributed to accelerated sea ice melt from 2007
425 to 2012 as ice is thinned by anthropogenic forcing. *Journal of Climate*, *0*(0), null. doi:
426 10.1175/JCLI-D-18-0783.1
- 427 Blanchard-Wrigglesworth, E., Armour, K. C., Bitz, C. M., & DeWeaver, E. (2011). Persis-
428 tence and inherent predictability of Arctic sea ice in a GCM ensemble and observations.
429 *Journal of Climate*, *24*(1), 231–250.
- 430 Blanchard-Wrigglesworth, E., Bitz, C., & Holland, M. (2011). Influence of initial conditions
431 and climate forcing on predicting Arctic sea ice. *Geophysical Research Letters*, *38*(18).
- 432 Blanchard-Wrigglesworth, E., & Bushuk, M. (2019). Robustness of Arctic sea-ice pre-
433 dictability in GCMs. *Climate Dynamics*, *52*(9-10), 5555–5566.
- 434 Blanchard-Wrigglesworth, E., Cullather, R., Wang, W., Zhang, J., & Bitz, C. (2015). Model
435 forecast skill and sensitivity to initial conditions in the seasonal Sea Ice Outlook.
436 *Geophysical Research Letters*, *42*(19), 8042–8048.
- 437 Blanchard-Wrigglesworth, E., & Ding, Q. (2019). Tropical and midlatitude impact on
438 seasonal polar predictability in the Community Earth System Model. *Journal of
439 Climate*, *32*(18), 5997–6014.
- 440 Bonan, D. B., Bushuk, M., & Winton, M. (2019). A spring barrier for regional predictions
441 of summer Arctic sea ice. *Geophysical Research Letters*, *46*(8), 5131–5140.
- 442 Bonan, D. B., Christian, J. E., & Christianson, K. (2019). Influence of North Atlantic
443 climate variability on glacier mass balance in Norway, Sweden and Svalbard. *Journal
444 of Glaciology*, *65*(252), 580–594.
- 445 Bushuk, M., Msadek, R., Winton, M., Vecchi, G., Yang, X., Rosati, A., & Gudgel, R. (2019).
446 Regional Arctic sea-ice prediction: potential versus operational seasonal forecast skill.

- 447 *Climate Dynamics*, 52(5-6), 2721–2743.
- 448 Bushuk, M., Msadek, R., Winton, M., Vecchi, G. A., Gudgel, R., Rosati, A., & Yang, X.
449 (2017). Skillful regional prediction of Arctic sea ice on seasonal timescales. *Geophysical*
450 *Research Letters*, 44(10), 4953–4964.
- 451 Castruccio, F. S., Ruprich-Robert, Y., Yeager, S. G., Danabasoglu, G., Msadek, R., & Del-
452 worth, T. L. (2019). Modulation of Arctic sea ice loss by atmospheric teleconnections
453 from Atlantic multidecadal variability. *Journal of Climate*, 32(5), 1419–1441.
- 454 Chevallier, M., Salas y Mélia, D., Voldoire, A., Déqué, M., & Garric, G. (2013). Seasonal
455 forecasts of the pan-Arctic sea ice extent using a GCM-based seasonal prediction
456 system. *Journal of Climate*, 26(16), 6092–6104.
- 457 Coats, S., Smerdon, J. E., Cook, B. I., & Seager, R. (2013). Stationarity of the trop-
458 ical pacific teleconnection to North America in CMIP5/PMIP3 model simulations.
459 *Geophysical Research Letters*, 40(18), 4927–4932.
- 460 Comiso, J. C., Meier, W. N., & Gersten, R. (2017). Variability and trends in the Arctic sea
461 ice cover: Results from different techniques. *Journal of Geophysical Research: Oceans*,
462 122(8), 6883–6900.
- 463 Comiso, J. C., Parkinson, C. L., Gersten, R., & Stock, L. (2008). Accelerated decline in the
464 Arctic sea ice cover. *Geophysical research letters*, 35(1).
- 465 Dätwyler, C., Neukom, R., Abram, N. J., Gallant, A. J., Grosjean, M., Jacques-Coper,
466 M., ... Villalba, R. (2018). Teleconnection stationarity, variability and trends of
467 the Southern Annular Mode (SAM) during the last millennium. *Climate dynamics*,
468 51(5-6), 2321–2339.
- 469 Day, J., Hawkins, E., & Tietsche, S. (2014). Will Arctic sea ice thickness initialization
470 improve seasonal forecast skill? *Geophysical Research Letters*, 41(21), 7566–7575.
- 471 Day, J., Tietsche, S., & Hawkins, E. (2014). Pan-Arctic and regional sea ice predictability:
472 Initialization month dependence. *Journal of Climate*, 27(12), 4371–4390.
- 473 Ding, Q., Schweiger, A., LHeureux, M., Battisti, D. S., Po-Chedley, S., Johnson, N. C., ...
474 others (2017). Influence of high-latitude atmospheric circulation changes on summer-
475 time Arctic sea ice. *Nature Climate Change*, 7(4), 289.
- 476 Ding, Q., Schweiger, A., LHeureux, M., Steig, E. J., Battisti, D. S., Johnson, N. C., ...
477 others (2019). Fingerprints of internal drivers of Arctic sea ice loss in observations
478 and model simulations. *Nature Geoscience*, 12(1), 28.
- 479 Ding, Q., Wallace, J. M., Battisti, D. S., Steig, E. J., Gallant, A. J., Kim, H.-J., & Geng, L.

- 480 (2014). Tropical forcing of the recent rapid Arctic warming in northeastern Canada
481 and Greenland. *Nature*, *509*(7499), 209.
- 482 Dirkson, A., Merryfield, W. J., & Monahan, A. (2017). Impacts of sea ice thickness initial-
483 ization on seasonal Arctic sea ice predictions. *Journal of Climate*, *30*(3), 1001–1017.
- 484 Eicken, H. (2013). Ocean science: Arctic sea ice needs better forecasts. *Nature*, *497*(7450),
485 431.
- 486 Ford, J. D., & Smit, B. (2004). A framework for assessing the vulnerability of communities in
487 the Canadian Arctic to risks associated with climate change. *Arctic*, *57*(4), 389–400.
- 488 Guemas, V., Blanchard-Wrigglesworth, E., Chevallier, M., Day, J. J., Déqué, M., Doblus-
489 Reyes, F. J., . . . others (2016). A review on Arctic sea-ice predictability and prediction
490 on seasonal to decadal time-scales. *Quarterly Journal of the Royal Meteorological*
491 *Society*, *142*(695), 546–561.
- 492 Hawkins, E., & Sutton, R. (2009). The potential to narrow uncertainty in regional climate
493 predictions. *Bulletin of the American Meteorological Society*, *90*(8), 1095–1108.
- 494 Hofstra, N., Haylock, M., New, M., Jones, P., & Frei, C. (2008). Comparison of six methods
495 for the interpolation of daily, European climate data. *Journal of Geophysical Research:*
496 *Atmospheres*, *113*(D21).
- 497 Holland, M. M., Bailey, D. A., & Vavrus, S. (2011). Inherent sea ice predictability in
498 the rapidly changing Arctic environment of the Community Climate System Model,
499 version 3. *Climate dynamics*, *36*(7-8), 1239–1253.
- 500 Hu, C., Yang, S., Wu, Q., Li, Z., Chen, J., Deng, K., . . . Zhang, C. (2016). Shifting El Niño
501 inhibits summer Arctic warming and Arctic sea-ice melting over the Canada Basin.
502 *Nature communications*, *7*, 11721.
- 503 Johannessen, O. M., Shalina, E. V., & Miles, M. W. (1999). Satellite evidence for an Arctic
504 sea ice cover in transformation. *Science*, *286*(5446), 1937–1939.
- 505 Jung, T., Gordon, N. D., Bauer, P., Bromwich, D. H., Chevallier, M., Day, J. J., . . . oth-
506 ers (2016). Advancing polar prediction capabilities on daily to seasonal time scales.
507 *Bulletin of the American Meteorological Society*, *97*(9), 1631–1647.
- 508 Kalnay, E., Kanamitsu, M., Kistler, R., Collins, W., Deaven, D., Gandin, L., . . . others
509 (1996). The NCEP/NCAR 40-year reanalysis project. *Bulletin of the American me-*
510 *teorological Society*, *77*(3), 437–472.
- 511 Kapsch, M.-L., Graverson, R. G., & Tjernström, M. (2013). Springtime atmospheric energy
512 transport and the control of Arctic summer sea-ice extent. *Nature Climate Change*,

- 513 3(8), 744.
- 514 Kay, J. E., Holland, M. M., & Jahn, A. (2011). Inter-annual to multi-decadal Arctic sea ice
515 extent trends in a warming world. *Geophysical Research Letters*, 38(15).
- 516 Kolstad, E., & Screen, J. (2019). Non-stationary relationship between autumn Arctic sea
517 ice and the winter North Atlantic Oscillation. *Geophysical Research Letters*.
- 518 Kwok, R., & Rothrock, D. (2009). Decline in Arctic sea ice thickness from submarine and
519 ICESat records: 1958–2008. *Geophysical Research Letters*, 36(15).
- 520 L’Heureux, M. L., Kumar, A., Bell, G. D., Halpert, M. S., & Higgins, R. W. (2008).
521 Role of the Pacific-North American (PNA) pattern in the 2007 Arctic sea ice decline.
522 *Geophysical Research Letters*, 35(20).
- 523 Maslanik, J., Stroeve, J., Fowler, C., & Emery, W. (2011). Distribution and trends in Arctic
524 sea ice age through spring 2011. *Geophysical Research Letters*, 38(13).
- 525 Meehl, G. A., Chung, C. T., Arblaster, J. M., Holland, M. M., & Bitz, C. M. (2018). Trop-
526 ical decadal variability and the rate of Arctic sea ice decrease. *Geophysical Research*
527 *Letters*, 45(20), 11–326.
- 528 Melia, N., Haines, K., & Hawkins, E. (2016). Sea ice decline and 21st century trans-Arctic
529 shipping routes. *Geophysical Research Letters*, 43(18), 9720–9728.
- 530 Merryfield, W., Lee, W.-S., Wang, W., Chen, M., & Kumar, A. (2013). Multi-system
531 seasonal predictions of Arctic sea ice. *Geophysical Research Letters*, 40(8), 1551–
532 1556.
- 533 Msadek, R., Vecchi, G., Winton, M., & Gudgel, R. (2014). Importance of initial conditions
534 in seasonal predictions of Arctic sea ice extent. *Geophysical Research Letters*, 41(14),
535 5208–5215.
- 536 Ogi, M., Yamazaki, K., & Wallace, J. M. (2010). Influence of winter and summer surface
537 wind anomalies on summer Arctic sea ice extent. *Geophysical Research Letters*, 37(7).
- 538 Olonscheck, D., Mauritsen, T., & Notz, D. (2019). Arctic sea-ice variability is primarily
539 driven by atmospheric temperature fluctuations. *Nature Geoscience*, 12(6), 430.
- 540 Petty, A., Schröder, D., Stroeve, J., Markus, T., Miller, J., Kurtz, N., . . . Flocco, D. (2017).
541 Skillful spring forecasts of September Arctic sea ice extent using passive microwave
542 sea ice observations. *Earth’s Future*, 5(2), 254–263.
- 543 Pizzolato, L., Howell, S. E., Dawson, J., Laliberté, F., & Copland, L. (2016). The influence
544 of declining sea ice on shipping activity in the Canadian Arctic. *Geophysical Research*
545 *Letters*, 43(23), 12–146.

- 546 Raible, C., Lehner, F., González-Rouco, J., & Fernández-Donado, L. (2014). Changing
547 correlation structures of the Northern Hemisphere atmospheric circulation from 1000
548 to 2100 AD. *Climate of the Past*, *10*(2), 537–550.
- 549 Rayner, N., Parker, D. E., Horton, E., Folland, C. K., Alexander, L. V., Rowell, D., ...
550 Kaplan, A. (2003). Global analyses of sea surface temperature, sea ice, and night
551 marine air temperature since the late nineteenth century. *Journal of Geophysical
552 Research: Atmospheres*, *108*(D14).
- 553 Rigor, I. G., & Wallace, J. M. (2004). Variations in the age of Arctic sea-ice and summer
554 sea-ice extent. *Geophysical Research Letters*, *31*(9).
- 555 Rothrock, D. A., Yu, Y., & Maykut, G. A. (1999). Thinning of the Arctic sea-ice cover.
556 *Geophysical Research Letters*, *26*(23), 3469–3472.
- 557 Schröder, D., Feltham, D. L., Flocco, D., & Tsamados, M. (2014). September Arctic sea-ice
558 minimum predicted by spring melt-pond fraction. *Nature Climate Change*, *4*(5), 353.
- 559 Screen, J. A., & Deser, C. (2019). Pacific Ocean variability influences the time of emergence
560 of a seasonally ice-free Arctic Ocean. *Geophysical Research Letters*, *46*(4), 2222–2231.
- 561 Screen, J. A., & Francis, J. A. (2016). Contribution of sea-ice loss to Arctic amplification
562 is regulated by Pacific Ocean decadal variability. *Nature Climate Change*, *6*(9), 856.
- 563 Serreze, M. C., Holland, M. M., & Stroeve, J. (2007). Perspectives on the Arctic’s shrinking
564 sea-ice cover. *science*, *315*(5818), 1533–1536.
- 565 Serreze, M. C., & Meier, W. N. (2018). The Arctic’s sea ice cover: trends, variability,
566 predictability, and comparisons to the Antarctic. *Annals of the New York Academy of
567 Sciences*.
- 568 Sigmond, M., Fyfe, J., Flato, G., Kharin, V., & Merryfield, W. (2013). Seasonal forecast skill
569 of Arctic sea ice area in a dynamical forecast system. *Geophysical Research Letters*,
570 *40*(3), 529–534.
- 571 Smith, K. L., Polvani, L. M., & Tremblay, L. B. (2018). The impact of stratospheric
572 circulation extremes on minimum Arctic sea ice extent. *Journal of Climate*, *31*(18),
573 7169–7183.
- 574 Stroeve, J., Holland, M. M., Meier, W., Scambos, T., & Serreze, M. (2007). Arctic sea ice
575 decline: Faster than forecast. *Geophysical research letters*, *34*(9).
- 576 Taylor, K. E., Stouffer, R. J., & Meehl, G. A. (2012). An overview of CMIP5 and the
577 experiment design. *Bulletin of the American Meteorological Society*, *93*(4), 485–498.
- 578 Tietsche, S., Day, J., Guemas, V., Hurlin, W., Keeley, S., Matei, D., ... Hawkins, E. (2014).

- 579 Seasonal to interannual Arctic sea ice predictability in current global climate models.
580 *Geophysical Research Letters*, *41*(3), 1035–1043.
- 581 Trenberth, K. E., Branstator, G. W., Karoly, D., Kumar, A., Lau, N.-C., & Ropelewski, C.
582 (1998). Progress during TOGA in understanding and modeling global teleconnections
583 associated with tropical sea surface temperatures. *Journal of Geophysical Research:*
584 *Oceans*, *103*(C7), 14291–14324.
- 585 Wallace, J. M., & Gutzler, D. S. (1981). Teleconnections in the geopotential height field
586 during the Northern Hemisphere winter. *Monthly Weather Review*, *109*(4), 784–812.
- 587 Walsh, J. E., Fetterer, F., Scott Stewart, J., & Chapman, W. L. (2017). A database for
588 depicting Arctic sea ice variations back to 1850. *Geographical Review*, *107*(1), 89–107.
- 589 Wang, L., Yuan, X., Ting, M., & Li, C. (2016). Predicting summer Arctic sea ice concentra-
590 tion intraseasonal variability using a vector autoregressive model. *Journal of Climate*,
591 *29*(4), 1529–1543.
- 592 Wang, W., Chen, M., & Kumar, A. (2013). Seasonal prediction of Arctic sea ice extent from
593 a coupled dynamical forecast system. *Monthly Weather Review*, *141*(4), 1375–1394.
- 594 Williams, J., Tremblay, B., Newton, R., & Allard, R. (2016). Dynamic preconditioning of
595 the minimum September sea-ice extent. *Journal of Climate*, *29*(16), 5879–5891.
- 596 Woodgate, R. A., Weingartner, T., & Lindsay, R. (2010). The 2007 Bering Strait oceanic
597 heat flux and anomalous Arctic sea-ice retreat. *Geophysical Research Letters*, *37*(1).
- 598 Wyllie-Echeverria, T., & Wooster, W. S. (1998). Year-to-year variations in Bering Sea
599 ice cover and some consequences for fish distributions. *Fisheries Oceanography*, *7*(2),
600 159–170.
- 601 Yeager, S. G., Karspeck, A. R., & Danabasoglu, G. (2015). Predicted slowdown in the rate
602 of Atlantic sea ice loss. *Geophysical Research Letters*, *42*(24), 10–704.